Letter

High-resolution polar Kerr effect studies of CsV_3Sb_5 and ScV_6Sn_6 below the charge order transition

David R. Saykin,[1,2,3] Qianni Jiang,[2,4] Zhaoyu Liu,[5] Chandra Shekhar,[6] Claudia Felser,[6] Jiun-Haw Chu,[5] and Aharon Kapitulnik[1,2,3,4,*]

[1]*Geballe Laboratory for Advanced Materials, Stanford University, Stanford, California 94305, USA*
[2]*Stanford Institute for Materials and Energy Sciences, SLAC National Accelerator Laboratory, 2575 Sand Hill Road, Menlo Park, California 94025, USA*
[3]*Department of Physics, Stanford University, Stanford, California 94305, USA*
[4]*Department of Applied Physics, Stanford University, Stanford, California 94305, USA*
[5]*Department of Physics, University of Washington, Seattle, Washington 98195, USA*
[6]*Max Planck Institute for Chemical Physics of Solids, 01187 Dresden, Germany*

(Received 6 November 2025; revised 30 March 2026; accepted 8 May 2026; published 1 June 2026)

We report high-resolution polar Kerr effect measurements on CsV_3Sb_5 and ScV_6Sn_6single crystals in search of signatures of the spontaneous polar Kerr effect (PKE) below the charge order transitions of these materials. Utilizing two separate zero-area loop Sagnac interferometers operating at 1550- and 830-nm wavelengths, we studied the temperature dependence of a possible PKE after training with the magnetic field. While a finite-field Kerr measurement yielded optical rotation expected from the Pauli susceptibility of the itinerant carriers, no signal was detected at zero field to within the noise floor limit of the apparatus of below ~100 nanorad. Simultaneous coherent reflection measurements confirm the sharpness of the charge order transition in the same optical volume as the Kerr measurements. The application of strain to reveal a hidden flux-ordered magnetic state did not result in a finite Kerr effect.

DOI: 10.1103/xfv5-3z9t

Introduction. Kagomé lattice-based quantum materials feature corner-sharing triangles arranged in a hexagonal cell that lead to a wide range of unique electronic phases controlled by correlations and topology (see, e.g., Refs. [1–3]). In particular, emerging flat bands and van Hove singularities promote strong electron-electron interactions and electron-phonon coupling that may result in structural instabilities as well as competing electronic orders such as charge density waves (CDWs), superconductivity, and nematicity. A particularly interesting pair of compounds to compare are CsV_3Sb_5, where a charge-density wave (CDW) state emerges below approximately $T_{CDW} = 94$ K, characterized by a lattice reconstruction within the vanadium plane [4], and ScV_6Sn_6, which exhibits a CDW state below $T_{CDW} = 92$ K, associated primarily with modulation of the Sc and Sn atoms along the c axis [5] (see Fig. 1). While CsV_3Sb_5 exhibits superconductivity at low temperatures ($T_c \lesssim 4$ K), ScV_6Sn_6 remains a normal metal with moderate residual resistivity of ~20 μΩ cm.

A lingering issue associated with kagomé systems exhibiting charge order transitions originates from the theoretical prediction of co-occurrence of time-reversal symmetry breaking (TRSB) associated with a flux-ordered magnetic state and the CDW transition [6–8]. This type of chiral flux phase represents an intriguing state of matter, potentially hosting exotic transport and optical responses due to nontrivial electronic topology and orbital magnetism. In particular, it has been suggested that different types of strain can affect "hidden" TRSB-originated effects [9–12], a property that needs further experimental scrutiny for the CsV_3Sb_5 and ScV_6Sn_6 systems.

Experimental evidence regarding TRSB in AV_3Sb_5 (A = Cs, Rb, K) metals has been controversial. Initial scanning tunneling microscopy (STM) studies have reported chirality switching of CDW peaks under a high applied magnetic field, indicative of a time-reversal-symmetry-broken

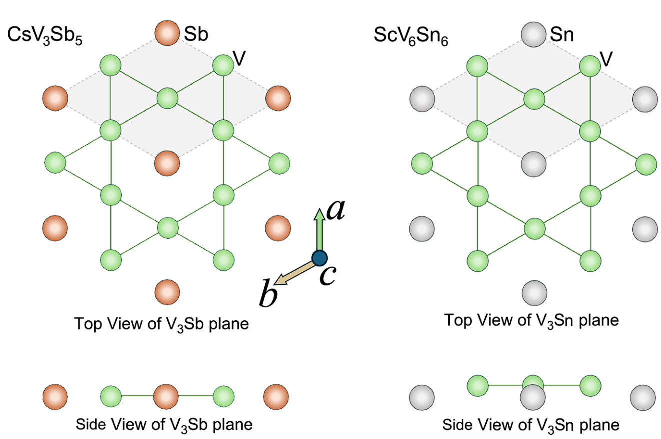

FIG. 1. Corner-sharing triangles of vanadium atoms constitute the Kagomé lattice planes of CsV_3Sb_5 (left) and ScV_6Sn_6 (right). Side views highlight the relative displacement of the vanadium and Sn planes in ScV_6Sn_6. The shaded area corresponds to the rhombus-shaped unit cell.

*Contact author: aharonk@stanford.edu

chiral state [13–15]. However, subsequent STM studies of CsV_3Sb_5 with spin-polarized tips found no evidence of chirality switching or local magnetic moments [16] challenging earlier interpretations. Similarly, an independent STM study of KV_3Sb_5 reported the absence of sensitivity of CDW peaks to the magnetic field [17], but at the same time a recent report on RbV_3Sb_5 has confirmed the possibility of chirality flipping with the sign of the magnetic field [12].

Muon spin relaxation (μSR) experiments have also provided conflicting results. Studies of CsV_3Sb_5 have observed enhanced internal magnetic fields below the CDW transition [18,19] and interpreted it as evidence of TRSB. Similar μSR evidence for hidden magnetism has been reported in ScV_6Sn_6 [20]. At the same time μSR experiments on KV_3Sb_5 [21] have attributed observed changes in relaxation rates at the CDW transition to nuclear rather than electronic fields, thus concluding that no evidence of TRSB is present. Indeed, a similar conclusion emerged in the studies of the pseudogap transition in the high-Tc cuprates when it was realized that, while μSR is not directly sensitive to charge order, it may sense its presence via the effect it has on the magnetic dipolar coupling of the muon with the host nuclei at zero- or low-magnetic fields [22,23].

Transport measurements have revealed an appearance of nonlinear-in-H behavior below the CDW transition in CsV_3Sb_5 and related compounds, which has been interpreted as a precursor to the anomalous Hall effect indicative of spontaneous orbital magnetism [24–27]. However, recent detailed studies of CsV_3Sb_5 have proposed an alternative explanation: these apparent anomalies could arise from high-mobility low-density Fermi pockets opening below T_{CDW} and specific Fermi surface reconstructions rather than from intrinsic TRSB phenomena [28,29].

Magneto-optic (MO) experiments have provided some of the most intriguing, yet contentious, results regarding TRSB. Early experiments [30,31] searching for either the magneto-optic polar Kerr effect (PKE) or its associated ellipticity, also known as reflective circular dichroism (RCD), have been performed through analysis of the polarization and amplitude of linearly polarized light reflected from CsV_3Sb_5 samples. Both experiments were judged to yield a very large effect, of order $\sim$50 μrad for PKE and $\sim$1 mrad for RCD signals, which would deem the MO response of CsV_3Sb_5 to be similar to that of hard ferromagnets [32]. Such a result would also be at odds with optical measurements, which have not found any special optical resonance associated with the CDW at the vicinity of $\sim$800 nm that could explain such a strong response [33,34]. By contrast, Saykin *et al.* [35] have performed high-resolution Sagnac interferometry measurements at a wavelength of 1550 nm, finding no observable spontaneous Kerr rotation within the 30-nrad noise floor over the $d = 10$ μm beam spot size. Furthermore, the center frequency of these measurements fell well within the full-width at half maximum of the most prominent Lorentz peak associated with the CDW transition centered at $\sim$1750 nm, thus expecting a strong magneto-optic response - if it existed. Farhang *et al.* [36] further tested the response of linearly polarized light at a 1550-nm wavelength and, similar to the Kerr and RCD measurements at 800 nm [31], also found unconventional specular optical rotation below the charge ordered state, thus further

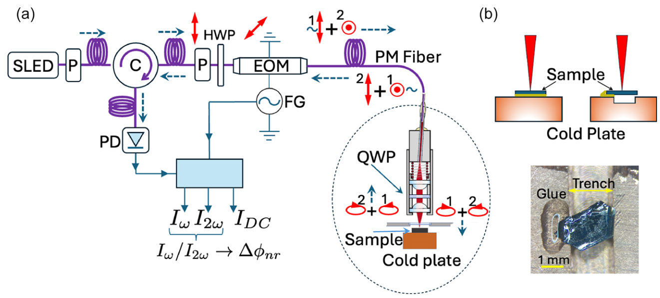

FIG. 2. Experimental setup. (a) Schematic of the Zero-Area Loop Sagnac Interferometer system. Light emitted from a superluminescent diode (SLED) is polarized (P) and then goes through a circulator (C) and is vertically polarized (P). A Half-wave plate rotates the polarization at 45° and only the vertical component is modulated at the electro-optic modulator (EOM) at frequency ω, controlled by a function generator (FG). Upon exiting the EOM, the two, now incoherent, components (marked as "1" and "2") are launched into the two axes of a polarization maintaining (PM) fiber. The two beams enter the probe end optics assembly (enlarged within the dashed-lined ellipse), where a quarter-wave plate (QWP) transforms the two linear polarizations into right and left circular polarizations. Upon reflection from the sample, the two beams exchange the circular polarization role. In the presence of birefringence, these polarizations become slightly elliptical, and in the presence of TRSB a nonreciprocal phase shift, $\Delta\phi_{nr}$, is acquired. Moving back in the same optical path, the two beams coherently combine at the detector and the output signal is analyzed to extract $\theta_K = \Delta\phi_{nr}$. (b) Top panel shows two ways of mounting a CsV_3Sb_5 crystal, either flat on the cold plate or over a trench, affixed at one side only, while the bottom panel shows a photo of a mounted sample over a trench.

forcing the need for more comprehensive true measurements of PKE and RCD in the range of 800- to 1550-nm wavelengths while taking extra care to strain effects.

In the present paper we reinforce our search for TRSB through searching for a finite PKE response in CsV_3Sb_5 by performing measurements using a newly constructed 830-nm zero-area Sagnac interferometer (ZALSI). We further perform similar measurements at both 1550- and 830-nm wavelengths on ScV_6Sn_6, where TRSB was similarly deduced from μSR [20] and Hall effect [26,27]measurements. Our primary result is that neither CsV_3Sb_5 nor ScV_6Sn_6 shows a discernible zero-field PKE signal to within $\sim$50 nrad. Additionally, uniaxial strain of magnitude $\pm 0.1\%$ does not induce spontaneous Kerr signals in CsV_3Sb_5, despite the significant strain sensitivity previously reported in transport [9,10] and, with the assumption that this system is similar in behavior to CsV_3Sb_5, STM results on RbV_3Sb_5[12]. Our findings significantly constrain the potential magnitude of the spontaneous and unstrained orbital flux phase and challenge theoretical models that predict large observable TRSB effects, particularly arguing for a large Kerr signal [37].

Methods. High-resolution measurement of magneto-optical Kerr response is enabled by utilizing a ZALSI, first reported by Xia *et al.* [38]. At the heart of the ZALSI [Fig. 2(a)] is a Sagnac loop [39] featuring two counterpropagating beams traveling along the two orthogonal axes of a $\sim$10-m polarization maintaining optical fiber. A quarter waveplate at the end of the fiber converts the two beams into right and left circularly polarized light that are focused onto a small interaction region on the sample. The reflected light beams are converted back to linear polarizations with exchanged linear polarization states, thus completing the loop in which both counterpropagating beams experience the exact same optical path. Owing to the reciprocity of the apparatus, a nonreciprocal phase shift, $\Delta\phi_{\rm nr}$, will appear at the detector only if time-reversal symmetry is broken through the interaction of the two circularly polarized beams with the sample. To extract $\Delta\phi_{\rm nr}$, the relative phase of the two counterpropagating beams is modulated at the proper frequency ω (see Supplemental Material [40]) such that the signals at 0ω, 1ω, and 2ω denoted as $I_{\rm DC}$, I_ω, and $I_{2\omega}$ can yield the Kerr signal through $\tan\theta_K = CI_\omega/I_{2\omega}$ (C is a known constant). In addition, both $I_{2\omega}$ and $I_{\rm DC}$, as well as their ratio, are a sensitive measure of any linear and/or circular birefringence effects, including reciprocal effects, present in the sample. For example, this mode of the ZALSI was previously used to detect the low-temperature orthorhombic to low-temperature tetragonal transition in lanthanum barium copper oxide with exquisite resolution [41]. For a detailed description of the apparatus, see, e.g., Kapitulnik *et al.* [42]. Some of our notable accomplishments include the study of TRSB in Sr_2RuO_4 [43] and UPt_3 [44], the discovery of the limit for ferromagnetism in thin $SrRuO_3$ films [45], the inverse proximity effect in ferromagnet/superconductor bilayers [46], and the subtle ferromagnetism beyond the dome in lanthanum cerium copper oxide $La_{2-x}Ce_xCuO_4$ cuprates [47].

High-quality single crystals of CsV_3Sb_5 were synthesized using the self-flux method. The flux is a eutectic Cs_xSb_y mixed with VSb_2 as described in Ref. [4], while single crystals of ScV_6Sn_6 were grown using the Sn-flux method, as previously reported [5], yielding hexagon-shaped single crystals.

Previous measurements on CsV_3Sb_5 have suggested that strain may alter the CDW transition and the subsequent emerging phases [10]. Thus, samples were mounted onto the cold finger in two different configurations. First directly attached to a flat cold plate and second only to one side of a trench carved in the cold plate [see Fig. 2(b)]. No difference in optical measurements was found in the two mounting configurations. However, to directly test the effect of strain on the Kerr results, samples were cut in the desired direction and then mounted on a "Razorbill" commercial cryogenic uniaxial strain cell, CS100. Following STM results on RbV_3Sb_5 [12], we also used a small magnetic field (±25 mT) to train the samples in the presence of uniaxial tensile or compressional stress in the a direction (see Fig. 1). Measurements were done while warming up the sample in zero-magnetic field at fixed applied strain.

Results and discussion. Overall, our ZALSI results on CsV_3Sb_5 and ScV_6Sn_6 follow the initial study on CsV_3Sb_5 [35], where recording $I_{\rm DC}$, I_ω, and $I_{2\omega}$ as a function of temperature and magnetic field training effects yields information about possible spontaneous PKE in the samples as well as tracking the CDW transition through the emergence of any birefringence effects (see Methods section). Figures 3(a) and 3(b) show data taken using a 1550-nm ZALSI. Similar to Ref. [35], a finite Kerr response appears in the presence of a magnetic field, similar to susceptibility measurements on this material, while at zero applied magnetic field, no PKE signal is observed through the CDW transition within the instrument resolution of ~30 to 50 nrad. Figures 3(c) and 3(d) show similar data, also at the 1550-nm wavelength, on ScV_6Sn_6 crystals. In Figs. 3(b) and 3(d), we also include, shown as a dashed line, the DC component of the reflectivity (in arbitrary units) measured simultaneously with the PKE, which reaffirms that the optical volume that we tested indeed underwent the CDW transition.

Following measurements using linearly polarized light at 800 nm [30,31], which reported a large Kerr response, up to 50 μrad, we used a 830-nm Sagnac system to search for such signals. Figures 4(a) and 4(b) show in-field and zero-field data on CsV_3Sb_5, while Figs. 4(c) and 4(d) show data on ScV_6Sn_6 crystals. While exhibiting somewhat larger error bars than when using the 1550-nm ZALSI, also here we see no evidence for spontaneous PKE for either kagomé system.

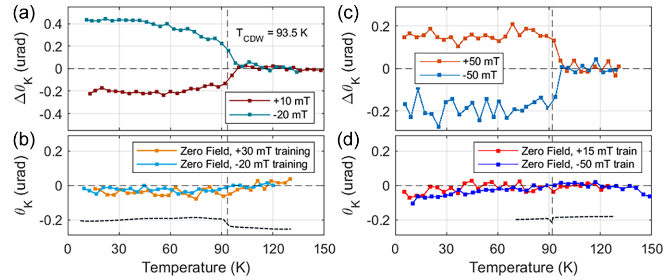

FIG. 3. Polar Kerr effect measurements at a 1550-nm wavelength: (a), (b) on CsV_3Sb_5 and (c), (d) on ScV_6Sn_6. Measurements in the magnetic field [panels (a) and (c)] track the transition with signal of order of the respective Pauli susceptibility [35]. Zero-field warmup measurements after training the sample in a field while cooling it through the CDW transition [panels (a) and (c)] show no evidence for a spontaneous Kerr effect (see text). Dashed lines in panels (b) and (d) track the DC component of the reflectivity (in arbitrary units) measured simultaneously with the PKE, which reaffirms that the optical volume that we tested indeed underwent the CDW transition.

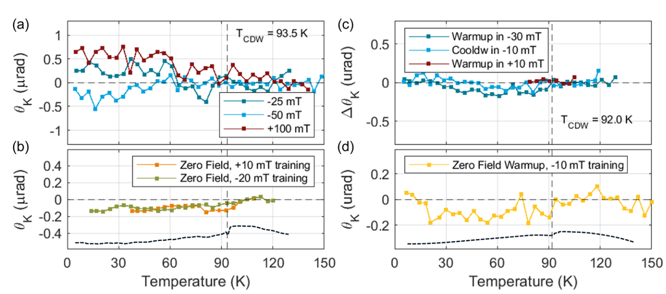

FIG. 4. Polar Kerr effect measurements at a 830-nm wavelength: (a), (b) on CsV_3Sb_5 and (c), (d) on ScV_6Sn_6. Similar to Fig. 3, measurements in the magnetic field [panels (a) and (c)] track the transition with signal of order of the respective Pauli susceptibility [35]. Zero-field warmup measurements after training the sample in a field while cooling it through the CDW transition [panels (a) and (c)] show no evidence for a spontaneous Kerr effect (see text). Dashed lines in panels (b) and (d) track the DC component of the reflectivity (in arbitrary units) measured simultaneously with the PKE, which reaffirms that the optical volume that we tested indeed underwent the CDW transition.

Comparing the 830-nm results to the 1550-nm results on CsV_3Sb_5, it is evident that the PKE response to a magnetic field at 1550 nm is several times larger than that at 830 nm, which is commensurate with optical measurements that identify a CDW-originated Lorentz peak at ~0.7 eV [33,34], with much breadth to include our 1550-nm measurements, but fades to no effect at ~800 nm. Signals at both 1550 and 830 nm are even smaller for ScV_6Sn_6, again commensurate with optical studies on this material [48].

From the nature of the ZALSI as an "absolute" test for a finite spontaneous PKE (that is, no subtraction of signals and/or external field modulations are needed), we conclude that there is no spontaneous PKE in either CsV_3Sb_5 or ScV_6Sn_6 in the vicinity of either a 1550-nm or a 800-nm wavelength to within the instrument's resolution of ~50 nrad, in contrast to measurements using analyses of reflected linearly polarized light [30,31]. Our results also respond to a recent study of a possible Kerr effect in CsV_3Sb_5 [37] suggesting to explain the discrepancies between measurements at the two wavelengths. Here we further note that, in general, if a particular resonance at a frequency ω_r could be a "best bet" to observe the effect, then at the minimum we should be able to observe the tails of that resonance with a typical $(\omega_r/\omega_0)^2$ resolution. For example, a ~1 mrad signal due to a resonance at $\hbar\omega_r = 1$ eV will be visible at $\hbar\omega_0 = 0.8$ eV (1550 nm) at a level of ~0.6 mrad or at ~0.4 mrad at $\hbar\omega_0 = 1.5$ eV (830 nm), both much larger than our instrument's resolution.

Nonetheless, taking the experiments that use linearly polarized light at face value, we show in the Supplemental Material [40] that a material possessing a combination of chirality and birefringence, but without time reversal symmetry breaking, will exhibit asymmetry in the reflecting polarization and circular dichroism associated with the off-diagonal elements of the reflection matrix, yet this asymmetry disappears if true circularly polarized light is used to test for polarization rotation. This simply reinforces the point that a net TRSB signal uniquely manifests itself as an asymmetry of the reflection amplitude and the phase of right vs left circularly polarized light [38,49,50]. The existence of an overall chiral structure in addition to the symmetry breaking due to the CDW transition also agrees with electronic magnetochiral anisotropy previously observed in CsV_3Sb_5 [9], as well as with the combination of chirality [13] and uniaxial charge order observed in STM [51] and optical [52] data.

While our results clearly forbid a net magnetic effect perpendicular to the surface of the sample, it cannot discern a possible underlying pure antiferromagnetic loop-current order that may exist in the material [10,52,53]. However, theories relying on loop-current order also predict strong sensitivity to strain, an important detail previously deduced from transport measurements [9,10]. Moreover, STM studies on the sister compound RbV_3Sb_5 [12] claimed evidence that the CDW relative intensity can be manipulated by inducing (anomalously large) strain through laser illumination with linearly polarized light along reciprocal lattice directions (which in real space will correspond to b and $\bar{b}$). They further argued that the same control can be achieved with a magnetic field applied in the z direction, similar to previous reports on CsV_3Sb_5 [14]. A simplified version of the analysis in Ref. [12], which displays coupling to both strain and magnetic field, is expected to be

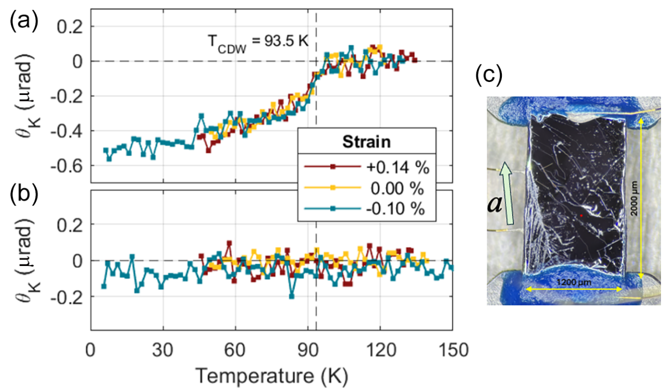

FIG. 5. Kerr signal in strained CsV_3Sb_5 at 1550 nm. (a) Kerr effect measured in an applied field of 50 mT, yielding Kerr signal similar to previous in-field measurements. (b) Zero-field warmup measurements after training in a field of 50 mT showing no discernible strain-induced signal through the CDW transition. (c) CsV_3Sb_5 crystal cut and mounted onto the strain cell. Crystal dimensions: 2 mm × 2 mm. An arrow marks the a direction of the crystal in the cell (see Fig. 1).

controlled by a two-component order parameter ψ, adding the following terms to the free energy of the CDW system:

$$\Delta\mathcal{F} = -\mathbf{m}\cdot\mathbf{H} + \psi_1(\varepsilon_{xx} - \varepsilon_{yy})H_z + \psi_2\varepsilon_{xy}H_z, \qquad (1)$$

where $\mathbf{m}$ is the uniform magnetization if it exists and the magnetic field is applied in the z direction. With the directions b and $\bar{b}$ equivalent, the second strain-field coupling term will induce a finite ψ_2 if we align the crystal along the a direction. This in turn will result in a finite Kerr effect. The authors further suggested that residual strain in the a direction induced in the crystals during experiments could result in a finite Kerr effect. While this is a plausible suggestion to explain small signals, it is an unlikely explanation for Kerr signals of the order of ~50 μrad (or larger) or much larger RCD observed in experiments [30,31]. Thus, expecting small signals, we searched for strain-induced Kerr signal using the Sagnac interferometer system.

Using the aforementioned "Razorbill" strain cell, we were able to apply uniaxial stress to the sample and cool it down through the CDW transition with tensile and compressive strains applied. A freshly cleaved surface was first exposed on the millimeter-size high-quality single crystal ensuring that the majority of the crystal, especially in the center region, was free from scratches. Thus, as seen in Fig. 5(c), only layering boundaries are visible in the majority of the crystal, which are typical for any layered bulk materials of this size. In our experiment, the light is focused to an ~20-μm^2 beam diameter. Reflectivity scans at both 300 K and low temperature (~40 K) were performed to find a flat region with good reflectivity, typically near the middle of the sample to ensure good strain transmission. No detectable built-in strain was found during cooldown without applying driving voltage on the piezoelectric transducer (PZT) that is minimal, certainly much smaller than the strain of ~0.1% that we report in this study or larger strains reported by Qian *et al.* [54] who used a similar apparatus. While in practice the applied strain is not purely uniaxial, we could estimate the perpendicular contribution from the

Poisson coefficients. In addition, T_{CDW} was monitored using a four-point transport probe on the back of the sample as well as the coherent reflection ratio measured with the Sagnac system, confirming that the sample remained unstrained to within the nominal transition point unless intentional strain was applied. In that case, the shifts were comparable to those found in Ref. [54].Following Eq. (1), we expect to see a finite signal which may change sign upon changing the strain direction. Figure 5 shows Kerr effect results with either tensile or compressive strains applied to the *a* direction (see Fig. 1). Analyzing the under-strain Kerr data we conclude that no discernible signal appears as a result of an applied uniaxial strain, either with an applied magnetic field or at zero field.

Conclusions. We report high-resolution polar Kerr effect measurements on CsV_3Sb_5 and ScV_6Sn_6 single crystals in search of signatures of the spontaneous polar Kerr effect (PKE) below the charge order transitions of these materials. Utilizing two zero-area loop Sagnac interferometers operating at 1550- and 830-nm wavelengths, we studied the temperature dependence of a possible PKE after training with the magnetic field. While a finite field Kerr measurement yielded optical rotation expected from the Pauli susceptibility of the itinerant carriers, no signal was detected at zero-field to within the noise floor limit of the apparatus at 30 nrad. Simultaneous coherent reflection measurements confirm the sharpness of the charge order transition in the same optical volume as the Kerr measurements. Application of strain to reveal a hidden flux-ordered magnetic state did not result in a finite Kerr effect. We further note that our measurements were typically taken down to $\sim$10 K, where no discernible signal could be detected at intermediate temperatures where we also observed anomalies in resistivity (see Supplemental Material [40]).

Focusing on CsV_3Sb_5, the above results need to be understood in the broader context of experiments on AV_3Sb_5. For example a detailed group theoretical analysis on the response of the CDW order parameter under electric and magnetic fields in materials with AV_3Sb_5 symmetry is given in Ref. [12]. Here the starting point is an antiferromagnetic (AFM)-ordered loop current state, which is argued to reveal itself after being similarly distorted by irradiation with linearly polarized light or the application of a magnetic field. In the present paper we attempted to carefully follow the recipe of Ref. [12], by applying direct distortion in the prescribed direction using a strain cell. However, no Kerr effect was observed as predicted in Ref. [12]. We therefore conclude that while an incipient AFM order may still exist, it must be immune to uniaxial strain or training in the magnetic field, at least down to $\sim$15 K. At the same time, we propose that below the CDW transition a chiral structure appears that is accompanied by breaking of rotational symmetry, which can explain linearly polarized light-based experiments and is compatible with all other experiments that claim a zero-field direct observation of TRSB.

Acknowledgments. The work at Stanford University was supported by the U.S. Department of Energy, Office of Science, Basic Energy Sciences, Division of Materials Sciences and Engineering, under Contract No. DE-AC02-76SF00515. CsV_3Sb_5 synthesis at the University of Washington was supported by the NSF MRSEC at UW (Grant No. DMR-2308979).

Data availability. The data that support the findings of this article are not publicly available upon publication because it is not technically feasible and/or the cost of preparing, depositing, and hosting the data would be prohibitive within the terms of this research project. The data are available from the authors upon reasonable request.

[1] S. D. Wilson and B. R. Ortiz, AV_3Sb_5 kagome superconductors, Nat. Rev. Mater. **9**, 420 (2024).

[2] Q. Wang, H. Lei, Y. Qi, and C. Felser, Intriguing kagome topological materials, npj Quantum Mater. **10**, 72 (2025).

[3] M. Li, H. Ma, R. Lou, and S. Wang, Electronic band structures of topological kagome materials, Chin. Phys. B **34**, 017101 (2025).

[4] B. R. Ortiz, S. M. L. Teicher, Y. Hu, J. L. Zuo, P. M. Sarte, E. C. Schueller, A. M. M. Abeykoon, M. J. Krogstad, S. Rosenkranz, R. Osborn, R. Seshadri, L. Balents, J. He, and S. D. Wilson, CsV_3Sb_5: A $\mathbb{Z}_2$ topological kagomé metal with a superconducting ground state, Phys. Rev. Lett. **125**, 247002 (2020).

[5] H. W. S. Arachchige, W. R. Meier, M. Marshall, T. Matsuoka, R. Xue, M. A. McGuire, R. P. Hermann, H. Cao, and D. Mandrus, Charge density wave in kagome lattice intermetallic ScV_6Sn_6, Phys. Rev. Lett. **129**, 216402 (2022).

[6] X. Feng, K. Jiang, Z. Wang, and J. Hu, Chiral flux phase in the kagomé superconductor AV_3Sb_5, Sci. Bull. **66**, 1384 (2021).

[7] M. M. Denner, R. Thomale, and T. Neupert, Analysis of charge order in the kagome metal AV_3Sb_5 (A = K, Rb, Cs), Phys. Rev. Lett. **127**, 217601 (2021).

[8] H. Li, Y. B. Kim, and H.-Y. Kee, Intertwined Van Hove singularities as a mechanism for loop current order in kagome metals, Phys. Rev. Lett. **132**, 146501 (2024).

[9] C. Guo, C. Putzke, S. Konyzheva, X. Huang, M. Gutierrez-Amigo, I. Errea, D. Chen, M. G. Vergniory, C. Felser, M. H. Fischer, T. Neupert, and P. J. W. Moll, Switchable chiral transport in charge-ordered kagome metal CsV_3Sb_5, Nature (London) **611**, 461 (2022).

[10] C. Guo, K. Wang, L. Zhang, C. Putzke, D. Chen, M. R. van Delft, S. Wiedmann, F. F. Balakirev, R. D. McDonald, M. Gutierrez-Amigo, M. Alkorta, I. Errea, M. G. Vergniory, T. Oka, R. Moessner, M. H. Fischer, T. Neupert, C. Felser, and P. J. W. Moll, Many-body interference in kagome crystals, Nature (London) **647**, 68 (2025).

[11] M. Alkorta, M. Gutierrez-Amigo, C. Guo, P. J. W. Moll, M. G. Vergniory, and I. Errea, Symmetry-broken charge-ordered ground state in CsV_3Sb_5 kagome metal, arXiv:2505.19686v2.

[12] Y. Xing, S. Bae, E. Ritz, F. Yang, T. Birol, A. N. Capa Salinas, B. R. Ortiz, S. D. Wilson, Z. Wang, R. M. Fernandes, and V. Madhavan, Optical manipulation of the charge-density-wave state in RbV_3Sb_5, Nature (London) **631**, 60 (2024).

[13] Z. Wang, Y.-X. Jiang, J.-X. Yin, Y. Li, G.-Y. Wang, H.-L. Huang, S. Shao, J. Liu, P. Zhu, N. Shumiya, M. S. Hossain, H. Liu, Y. Shi, J. Duan, X. Li, G. Chang, P. Dai, Z. Ye, G. Xu, Y. Wang, *et al.*, Electronic nature of chiral charge order in the kagomé superconductor CsV_3Sb_5, Phys. Rev. B **104**, 075148 (2021).

[14] Y.-X. Jiang, J.-X. Yin, M. M. Denner, N. Shumiya, B. R. Ortiz, G. Xu, Z. Guguchia, J. He, M. S. Hossain, X. Liu, J. Ruff, L. Kautzsch, S. S. Zhang, G. Chang, I. Belopolski, Q. Zhang, T. A. Cochran, D. Multer, M. Litskevich, Z.-J. Cheng, *et al.*, Unconventional chiral charge order in kagomé superconductor KV_3Sb_5, Nat. Mater. **20**, 1353 (2021).

[15] N. Shumiya, M. S. Hossain, J.-X. Yin, Y.-X. Jiang, B. R. Ortiz, H. Liu, Y. Shi, Q. Yin, H. Lei, S. S. Zhang, G. Chang, Q. Zhang, T. A. Cochran, D. Multer, M. Litskevich, Z.-J. Cheng, X. P. Yang, Z. Guguchia, S. D. Wilson, and M. Z. Hasan, Intrinsic nature of chiral charge order in the kagomé superconductor RbV_3Sb_5, Phys. Rev. B **104**, 035131 (2021).

[16] H. Li, S. Wan, H. Li, Q. Li, Q. Gu, H. Yang, Y. Li, Z. Wang, Y. Yao, and H.-H. Wen, No observation of chiral flux current in the topological kagome metal CsV_3Sb_5, Phys. Rev. B **105**, 045102 (2022).

[17] H. Li, H. Zhao, B. R. Ortiz, T. Park, M. Ye, L. Balents, Z. Wang, S. D. Wilson, and I. Zeljkovic, Rotation symmetry breaking in the normal state of a kagome superconductor KV_3Sb_5, Nat. Phys. **18**, 265 (2022).

[18] R. Khasanov, D. Das, R. Gupta, C. Mielke, M. Elender, Q. Yin, Z. Tu, C. Gong, H. Lei, E. T. Ritz, R. M. Fernandes, T. Birol, Z. Guguchia, and H. Luetkens, Time-reversal symmetry broken by charge order in CsV_3Sb_5, Phys. Rev. Res. **4**, 023244 (2022).

[19] Z. Shan, P. K. Biswas, S. K. Ghosh, T. Tula, A. D. Hillier, D. Adroja, S. Cottrell, G.-H. Cao, Y. Liu, X. Xu, Y. Song, H. Yuan, and M. Smidman, Muon spin relaxation study of the layered kagome superconductor CsV_3Sb_5, Phys. Rev. Res. **4**, 033145 (2022).

[20] Z. Guguchia, D. Gawryluk, S. Shin, Z. Hao, C. Mielke III, D. Das, I. Plokhikh, L. Liborio, J. K. Shenton, Y. Hu, *et al.*, Hidden magnetism uncovered in a charge ordered bilayer kagome material ScV_6Sn_6, Nat. Commun. **14**, 7796 (2023).

[21] E. M. Kenney, B. R. Ortiz, C. Wang, S. D. Wilson, and M. J. Graf, Absence of local moments in the kagome metal KV_3Sb_5 as determined by muon spin spectroscopy, J. Phys.: Condens. Matter **33**, 235801 (2021).

[22] J. E. Sonier, J. H. Brewer, R. F. Kiefl, R. H. Heffner, K. F. Poon, S. L. Stubbs, G. D. Morris, R. I. Miller, W. N. Hardy, R. Liang, D. A. Bonn, J. S. Gardner, C. E. Stronach, and N. J. Curro, Correlations between charge ordering and local magnetic fields in overdoped $YBa_2Cu_3O_{6+x}$, Phys. Rev. B **66**, 134501 (2002).

[23] J. Sonier, Charge order, superconducting correlations, and positive muons, J. Magn. Magn. Mater. **376**, 20 (2015).

[24] F. H. Yu, T. Wu, Z. Y. Wang, B. Lei, W. Z. Zhuo, J. J. Ying, and X. H. Chen, Concurrence of anomalous Hall effect and charge density wave in a superconducting topological kagomé metal, Phys. Rev. B **104**, L041103 (2021).

[25] S.-Y. Yang, Y. Wang, B. R. Ortiz, D. Liu, J. Gayles, E. Derunova, R. Gonzalez-Hernandez, L. Šmejkal, Y. Chen, S. S. P. Parkin, S. D. Wilson, E. S. Toberer, T. McQueen, and M. N. Ali, Giant, unconventional anomalous Hall effect in the metallic frustrated magnet candidate, KV_3Sb_5, Sci. Adv. **6**, eabb6003 (2020).

[26] C. Yi, X. Feng, N. Kumar, C. Felser, and C. Shekhar, Tuning charge density wave of kagome metal ScV_6Sn_6, New J. Phys. **26**, 052001 (2024).

[27] S. Mozaffari, W. R. Meier, R. P. Madhogaria, N. Peshcherenko, S.-H. Kang, J. W. Villanova, H. W. S. Arachchige, G. Zheng, Y. Zhu, K.-W. Chen, K. Jenkins, D. Zhang, A. Chan, L. Li, M. Yoon, Y. Zhang, and D. G. Mandrus, Universal sublinear resistivity in vanadium kagome materials hosting charge density waves, Phys. Rev. B **110**, 035135 (2024).

[28] S. Liu, M. Roppongi, M. Kimata, K. Ishihara, R. Grasset, M. Konczykowski, B. R. Ortiz, S. D. Wilson, K. Yoshimi, T. Shibauchi, and K. Hashimoto, Impact of tiny Fermi pockets with extremely high mobility on the Hall anomaly in the kagome metal CsV_3Sb_5, Phys. Rev. Lett. **135**, 056502 (2025).

[29] A. E. Koshelev, R. Chapai, D. Y. Chung, J. F. Mitchell, and U. Welp, Origin of anomalous magnetotransport in kagome superconductors AV_3Sb_5 (A = K,Rb,Cs), Phys. Rev. B **110**, 024512 (2024).

[30] Q. Wu, Z. X. Wang, Q. M. Liu, R. S. Li, S. X. Xu, Q. W. Yin, C. S. Gong, Z. J. Tu, H. C. Lei, T. Dong, and N. L. Wang, Simultaneous formation of two-fold rotation symmetry with charge order in the kagome superconductor CsV_3Sb_5 by optical polarization rotation measurement, Phys. Rev. B **106**, 205109 (2022).

[31] Y. Xu, Z. Ni, Y. Liu, B. R. Ortiz, Q. Deng, S. D. Wilson, B. Yan, L. Balents, and L. Wu, Three-state nematicity and magneto-optical Kerr effect in the charge density waves in kagome superconductors, Nat. Phys. **18**, 1470 (2022).

[32] P. Oppeneer, Magneto-optical Kerr spectra, Handb. Magn. Mater. **13**, 229 (2001).

[33] E. Uykur, B. R. Ortiz, O. Iakutkina, M. Wenzel, S. D. Wilson, M. Dressel, and A. A. Tsirlin, Low-energy optical properties of the nonmagnetic kagomé metal CsV_3Sb_5, Phys. Rev. B **104**, 045130 (2021).

[34] X. Zhou, Y. Li, X. Fan, J. Hao, Y. Dai, Z. Wang, Y. Yao, and H.-H. Wen, Origin of charge density wave in the kagome metal CsV_3Sb_5 as revealed by optical spectroscopy, Phys. Rev. B **104**, L041101 (2021).

[35] D. R. Saykin, C. Farhang, E. D. Kountz, D. Chen, B. R. Ortiz, C. Shekhar, C. Felser, S. D. Wilson, R. Thomale, J. Xia, and A. Kapitulnik, High resolution polar Kerr effect studies of CsV_3Sb_5: Tests for time-reversal symmetry breaking below the charge-order transition, Phys. Rev. Lett. **131**, 016901 (2023).

[36] C. Farhang, J. Wang, B. R. Ortiz, S. D. Wilson, and J. Xia, Unconventional specular optical rotation in the charge ordered state of kagome metal CsV_3Sb_5, Nat. Commun. **14**, 5326 (2023).

[37] H.-T. Liu, J. Huang, T. Zhou, and W. Huang, Constraints on the orbital flux phase in AV_3Sb_5 from the polar Kerr effect, Phys. Rev. B **111**, L041109 (2025).

[38] J. Xia, P. T. Beyersdorf, M. M. Fejer, and A. Kapitulnik, Modified Sagnac interferometer for high-sensitivity magneto-optic measurements at cryogenic temperatures, Appl. Phys. Lett. **89**, 062508 (2006).

[39] G. Sagnac, L'éther lumineux démontré par l'effet du vent relatif d'éther dans un interféromètre en rotation uniforme, Comptes Rendus **157**, 708 (1913).

[40] See Supplemental Material at http://link.aps.org/supplemental/10.1103/xfv5-3z9t for details on the device characterization and data analysis, which includes Refs. [55–60].

[41] H. Karapetyan, M. Hücker, G. D. Gu, J. M. Tranquada, M. M. Fejer, J. Xia, and A. Kapitulnik, Magneto-optical measurements of a cascade of transitions in superconducting $La_{1.875}Ba_{0.125}CuO_4$ single crystals, Phys. Rev. Lett. **109**, 147001 (2012).

[42] A. Kapitulnik, J. Xia, E. Schemm, and A. Palevski, Polar Kerr effect as probe for time-reversal symmetry breaking in unconventional superconductors, New J. Phys. **11**, 055060 (2009).

[43] J. Xia, Y. Maeno, P. T. Beyersdorf, M. M. Fejer, and A. Kapitulnik, High resolution polar Kerr effect measurements of Sr_2RuO_4: Evidence for broken time-reversal symmetry in the superconducting state, Phys. Rev. Lett. **97**, 167002 (2006).

[44] E. R. Schemm, W. J. Gannon, C. M. Wishne, W. P. Halperin, and A. Kapitulnik, Observation of broken time-reversal symmetry in the heavy-fermion superconductor UPt_3, Science **345**, 190 (2014).

[45] J. Xia, W. Siemons, G. Koster, M. R. Beasley, and A. Kapitulnik, Critical thickness for itinerant ferromagnetism in ultrathin films of $SrRuO_3$, Phys. Rev. B **79**, 140407(R) (2009).

[46] J. Xia, V. Shelukhin, M. Karpovski, A. Kapitulnik, and A. Palevski, Inverse proximity effect in superconductor-ferromagnet bilayer structures, Phys. Rev. Lett. **102**, 087004 (2009).

[47] T. Sarkar, D. S. Wei, J. Zhang, N. R. Poniatowski, P. R. Mandal, A. Kapitulnik, and R. L. Greene, Ferromagnetic order beyond the superconducting dome in a cuprate superconductor, Science **368**, 532 (2020).

[48] T. Hu, H. Pi, S. Xu, L. Yue, Q. Wu, Q. Liu, S. Zhang, R. Li, X. Zhou, J. Yuan, D. Wu, T. Dong, H. Weng, and N. Wang, Optical spectroscopy and band structure calculations of the structural phase transition in the vanadium-based kagome metal ScV_6Sn_6, Phys. Rev. B **107**, 165119 (2023).

[49] S. Spielman, K. Fesler, C. B. Eom, T. H. Geballe, M. M. Fejer, and A. Kapitulnik, Test for nonreciprocal circular birefringence in $YBa_2Cu_3O_7$ thin films as evidence for broken time-reversal symmetry, Phys. Rev. Lett. **65**, 123 (1990).

[50] B. I. Halperin, The hunt for anyon superconductivity, in *The Physics and Chemistry of Oxide Superconductors*, edited by Y. Iye and H. Yasuoka (Springer, Berlin, 1992), pp. 439–450.

[51] L. Nie, K. Sun, W. Ma, D. Song, L. Zheng, Z. Liang, P. Wu, F. Yu, J. Li, M. Shan, D. Zhao, S. Li, B. Kang, Z. Wu, Y. Zhou, K. Liu, Z. Xiang, J. Ying, Z. Wang, T. Wu, *et al.*, Charge-density-wave-driven electronic nematicity in a kagome superconductor, Nature (London) **604**, 59 (2022).

[52] M. H. Christensen, T. Birol, B. M. Andersen, and R. M. Fernandes, Loop currents in AV_3Sb_5 kagome metals: Multipolar and toroidal magnetic orders, Phys. Rev. B **106**, 144504 (2022).

[53] F. Grandi, A. Consiglio, M. A. Sentef, R. Thomale, and D. M. Kennes, Theory of nematic charge orders in kagome metals, Phys. Rev. B **107**, 155131 (2023).

[54] T. Qian, M. H. Christensen, C. Hu, A. Saha, B. M. Andersen, R. M. Fernandes, T. Birol, and N. Ni, Revealing the competition between charge density wave and superconductivity in CsV_3Sb_5 through uniaxial strain, Phys. Rev. B **104**, 144506 (2021).

[55] P. S. Pershan, Magneto-optical effects, J. Appl. Phys. **38**, 1482 (1967).

[56] E. A. Stern, J. C. McGroddy, and W. E. Harte, Polar reflection Faraday effect in metals, Phys. Rev. **135**, A1306 (1964).

[57] L. Uba, S. Uba, and V. N. Antonov, Magneto-optical Kerr spectroscopy of noble metals, Phys. Rev. B **96**, 235132 (2017).

[58] L. Yu, C. Wang, Y. Zhang, M. Sander, S. Ni, Z. Lu, S. Ma, Z. Wang, Z. Zhao, H. Chen, K. Jiang, Y. Zhang, H. Yang, F. Zhou, X. Dong, S. L. Johnson, M. J. Graf, J. Hu, H.-J. Gao, and Z. Zhao, Evidence of a hidden flux phase in the topological kagomé metal CsV_3Sb_5, arXiv:2107.10714.

[59] A. Kapitulnik, Notes on constraints for the observation of polar Kerr effect in complex materials, Phys. B (Amsterdam, Neth.) **460**, 151 (2015).

[60] J. C. McGroddy, A. J. McAlister, and E. A. Stern, Polar reflection Faraday effect in silver and gold, Phys. Rev. **139**, A1844 (1965).